Free-Energy Perturbation, Thermodynamic Integration, Potential of Mean Force

(+working examples on chemical reactivity)

Lubomír Rulíšek, Martin Srnec

Institute of Organic Chemistry and Biochemistry AS CR

J. Heyrovský Institute of Physical Chemistry AS CR, Prague, Czech Republic

Outline

Simulations of Thermodynamic Properties
- Free-Energy Perturbation
- Thermodynamic Integration
- Potential of Mean Force

Working Examples on Chemical Reactivity
- Computational Investigations of Asymmetric Organocatalysis
- Divergent Pathways and Competitive Mechanisms of Metathesis Reactions between 3-Arylprop-2-ynyl esters and Aldehydes

Explicit Models for Condensed Phases

Partition function

$$Q = \int\int e^{-E(\mathbf{q},\mathbf{p})/k_B T}\, d\mathbf{q}d\mathbf{p}$$

Statistical Thermodynamics (Lecture 5)

$$U = k_B T^2 \left(\frac{\partial \ln Q}{\partial T}\right)_V$$

$$A = -k_B T \ln Q$$

$$P = k_B T \left(\frac{\partial \ln Q}{\partial V}\right)_T$$

$$S = k_B T \left(\frac{\partial \ln Q}{\partial T}\right)_V + k_B \ln Q$$

$$H = U + PV$$

$$G = H - TS$$

We may rewrite *U* as

$$U = \frac{\iint E(\mathbf{q}, \mathbf{p}) e^{-E(\mathbf{q},\mathbf{p})/k_\mathrm{B}T} d\mathbf{q} d\mathbf{p}}{\iint e^{-E(\mathbf{q},\mathbf{p})/k_\mathrm{B}T} d\mathbf{q} d\mathbf{p}}$$

$$= \iint E(\mathbf{q}, \mathbf{p}) P(\mathbf{q}, \mathbf{p}) d\mathbf{q} d\mathbf{p}$$

Carrying Monte Carlo or MD

$$\langle U \rangle_\mathrm{B} - \langle U \rangle_\mathrm{A} = \frac{1}{M_\mathrm{B}} \sum_i^{M_\mathrm{B}} E_i - \frac{1}{M_\mathrm{A}} \sum_i^{M_\mathrm{A}} E_i$$

$$= \langle E \rangle_\mathrm{B} - \langle E \rangle_\mathrm{A}$$

Analogously, for *A*

$$A = k_B T \ln \frac{1}{Q}$$

$$= k_B T \ln \left[\frac{\iint e^{E(\mathbf{q},\mathbf{p})/k_B T} e^{-E(\mathbf{q},\mathbf{p})/k_B T} d\mathbf{q} d\mathbf{p}}{\iint e^{-E(\mathbf{q},\mathbf{p})/k_B T} d\mathbf{q} d\mathbf{p}} \right]$$

$$= k_B T \ln \left[\iint e^{E(\mathbf{q},\mathbf{p})/k_B T} P(\mathbf{q},\mathbf{p}) d\mathbf{q} d\mathbf{p} \right]$$

Carrying Monte Carlo or MD

$$\langle A \rangle_B - \langle A \rangle_A = k_B T \ln \left(\frac{1}{M_B} \sum_i^{M_B} e^{E_i/k_B T} \right) - k_B T \ln \left(\frac{1}{M_A} \sum_i^{M_A} e^{E_i/k_B T} \right)$$

$$= k_B T \ln \left\langle e^{E/k_B T} \right\rangle_B - k_B T \ln \left\langle e^{E/k_B T} \right\rangle_A$$

$$= k_B T \ln \left(\frac{\left\langle e^{E/k_B T} \right\rangle_B}{\left\langle e^{E/k_B T} \right\rangle_A} \right)$$

Free Energy Perturbation (Zwanzig, 1954)

$$\langle A \rangle_B - \langle A \rangle_A = k_B T \ln \langle e^{(E_B - E_A)/k_B T} \rangle_A$$

Example: HCN → HNC reaction
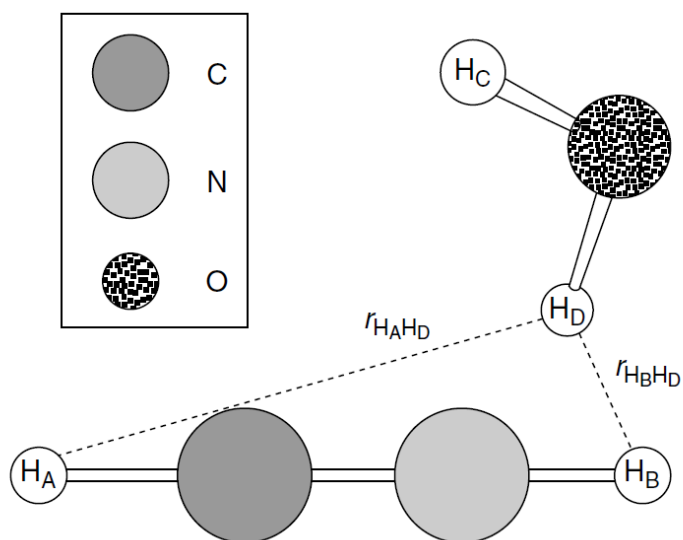
In practice, a simulation windows for each coupling parameter

$$E(\lambda) = \lambda E_{\mathrm{B}} + (1 - \lambda) E_{\mathrm{A}}$$

$$\langle A \rangle_{\mathrm{B}} - \langle A \rangle_{\mathrm{A}} = \sum_{\lambda=0}^{1} k_{\mathrm{B}} T \ln \left\langle e^{(E_{\lambda+d\lambda} - E_{\lambda})/k_{\mathrm{B}}T} \right\rangle_{\lambda}$$
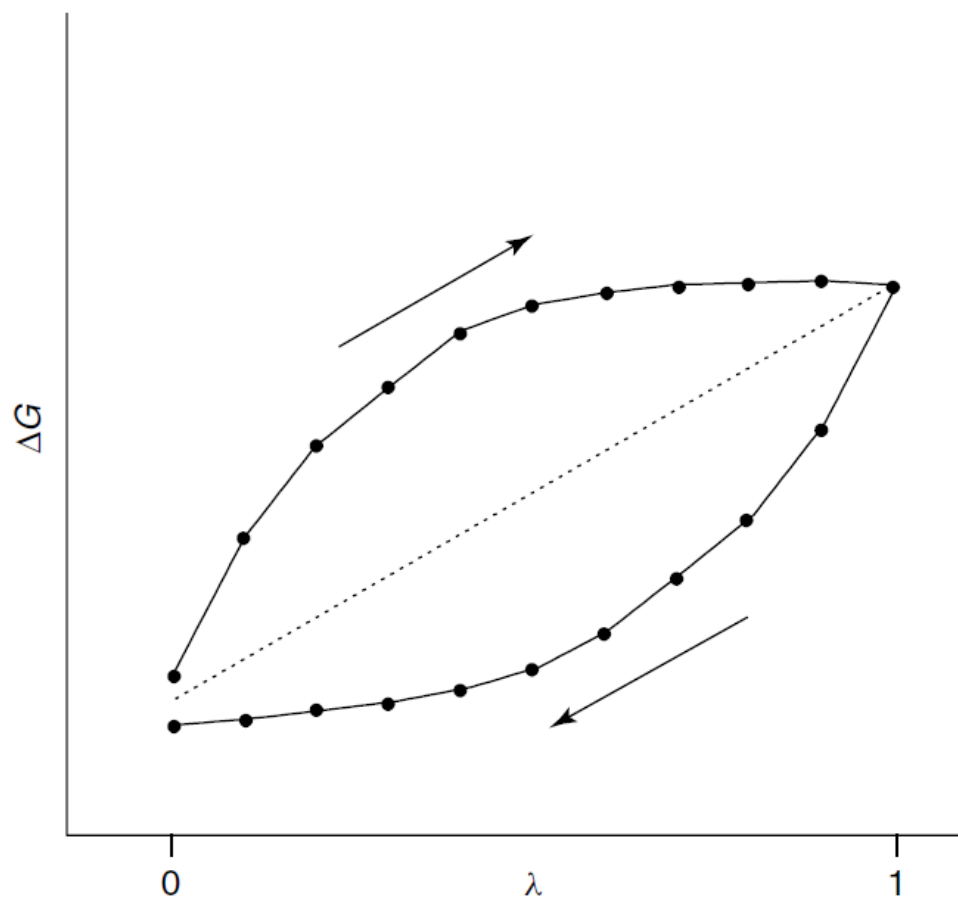
Figure 12.2 A typical FEP diagram showing the free-energy change in the forward (above) and reverse (below) directions for a λ-coupled mutation

Slow Growth Method

$$\langle A \rangle_B - \langle A \rangle_A = \lim_{d\lambda \to 0} \sum_{\lambda=0}^{1} k_B T \ln \left\langle 1 + \frac{(E_{\lambda+d\lambda} - E_\lambda)}{k_B T} \right\rangle_\lambda$$

$$\langle A \rangle_B - \langle A \rangle_A = \lim_{d\lambda \to 0} \sum_{\lambda=0}^{1} k_B T \left\langle \frac{(E_{\lambda+d\lambda} - E_\lambda)}{k_B T} \right\rangle_\lambda$$

$$= \lim_{d\lambda \to 0} \sum_{\lambda=0}^{1} \langle (E_{\lambda+d\lambda} - E_\lambda) \rangle_\lambda$$

$$= \lim_{d\lambda \to 0} \sum_{\lambda=0}^{1} (E_{\lambda+d\lambda} - E_\lambda)$$

Thermodynamic Integration

$$\langle A \rangle_B - \langle A \rangle_A = \lim_{d\lambda \to 0} \sum_{\lambda=0}^{1} \langle (E_{\lambda+d\lambda} - E_\lambda) \rangle_\lambda$$

$$= \lim_{\Delta\lambda \to 0} \sum_{\lambda=0}^{1} \left\langle \frac{(E_{\lambda+\Delta\lambda} - E_\lambda)}{\Delta\lambda} \right\rangle_\lambda \Delta\lambda$$

$$= \int_0^1 \left\langle \frac{\partial E}{\partial \lambda} \right\rangle_\lambda d\lambda$$

$$\approx \sum_{\lambda=0}^{1} \left\langle \frac{\partial E}{\partial \lambda} \right\rangle_\lambda \Delta\lambda$$

Potential of Mean Force

En Route to Quantitative Accuracy (~2 kcal.mol^{-1}) in "Computational Catalysis"

Challenges in Computational Homogeneous Catalysis

Accuracy of TS barriers (electronic structure)

Solvation Effects

Conformational Complexity

Nuclear Quantum Effects

ÚOCHB AV ČR

Asymmetric Allylation of Aldehydes with Allyltrichlorosilanes

reaction region

representative catalyst (Lewis base)
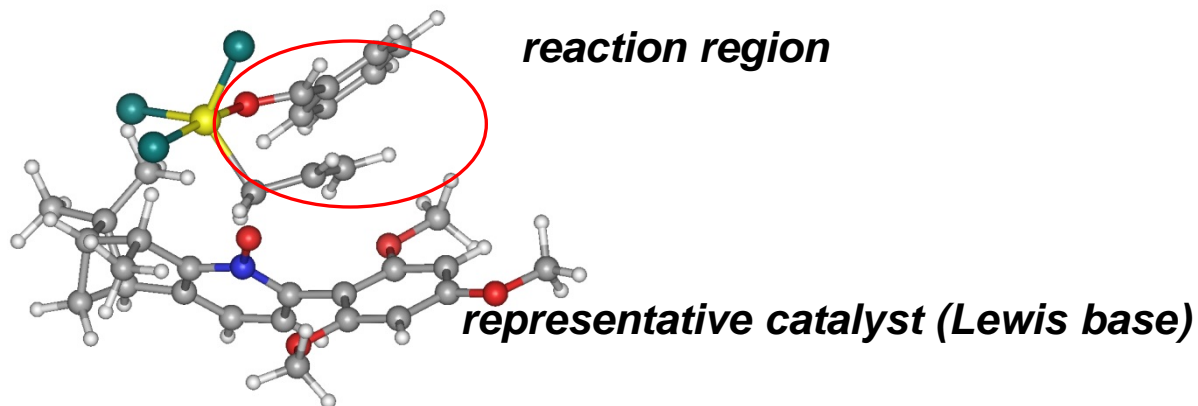
- ➢ **chiral phosphoramides (Denmark, 1994)**
- ➢ **axially chiral biquinoline *N,N'*-dioxide (Nakajima)**
- ➢ **bipyridine *N,N'*-dioxides and *N,N'N''*-trioxides (Hayashi, Kotora, Kwong, …)**
- ➢ **pyridine-derived *N*-monooxides (Kočovský, Malkov)**
- ➢ **"non-pyridine-type" *N*-monooxide derived from proline (Hoveyda)**
- ➢ ***N*-oxides derived from tetrahydroisoquinolines (Govender)**
- ➢ **sulfoxides, sulfonamides, phosphine oxides (BINAPO), dinitrones,…**

Computational ingredients:

Conformational Complexity, Dispersion/Solvation Effects, Entropic Effects

ÚOCHB AV ČR

Scheme 2. Mechanistic Dichotomy in the Coupling of Allyltrichlorosilane with Benzaldehyde Catalyzed By (S)-1b[20]
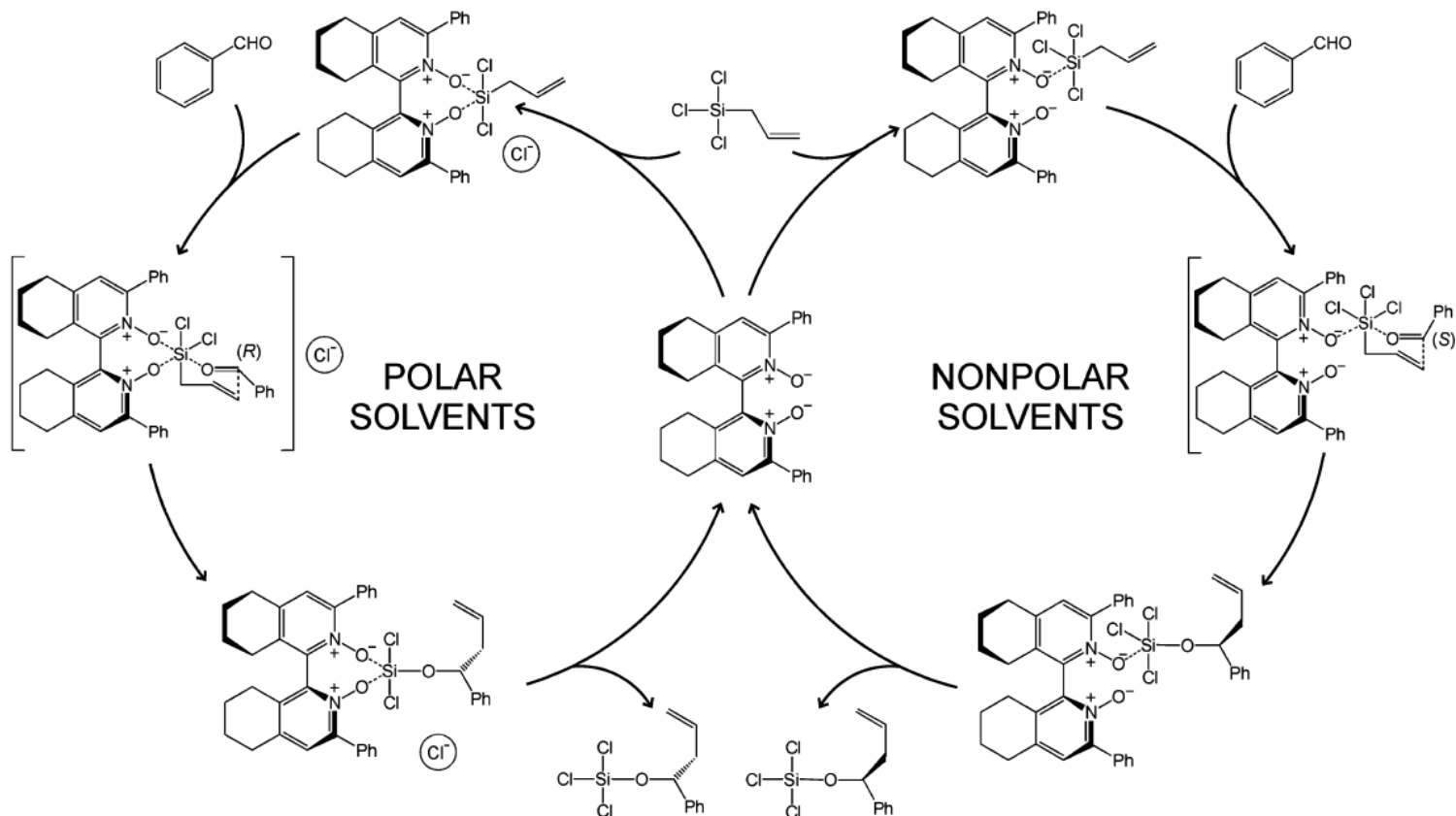
Ducháčková, L; Kadlčíková, A.; Kotora, M. ; Roithová, J.: Oxygen Superbases as Polar Binding Pockets in Nonpolar Solvents. *J. Am. Chem. Soc.* **2010**, *132*, 12660.

Kadlčíková, A.; Valterová, I.; Ducháčková, L; Roithová, J.; Kotora, M.: Lewis Base Catalyzed Enantioselective Allylation of alpha,beta-Unsaturated Aldehydes. *Chem. Eur. J.* **2010**, *16*, 9442.

Hrdina, R.; Opekar, F.; Roithová, J.; Kotora, M.: *Chem. Commun.* **2009**, 2314.

Dissociative (Cationic)/Associative (Mechanism) Solvent-Dependent Enantionselectivity

Table 1 Conductivity measurements

Entry	Solvent[a]	Composition	Conductivity/mV
1	MeCN	**1**	1560
2	MeCN	AllylSiCl$_3$	1510
3	MeCN	**1** + AllylSiCl$_3$	1780
4	MeCN[b]	AllylSiCl$_3$	1560
5	MeCN[b]	**1** + AllylSiCl$_3$	2100
6	CH$_2$Cl$_2$	AllylSiCl$_3$	188
7	CH$_2$Cl$_2$	**1** + AllylSiCl$_3$	458
8	PhCl	AllylSiCl$_3$	55
9	PhCl	**1** + AllylSiCl$_3$	57
10	EtOAc	AllylSiCl$_3$	62
11	EtOAc	**1** + AllylSiCl$_3$	63

[a] 0.0112 mmol ml^{-1} unless otherwise noted. [b] 0.0224 mmol ml^{-1}.

Hrdina, R.; Opekar, F.; Roithová, J.; Kotora, M.: *Chem. Commun.* **2009**, 2314.

(Possibly) New Mechanism (Polar-pocket or "Enzymatic-like")
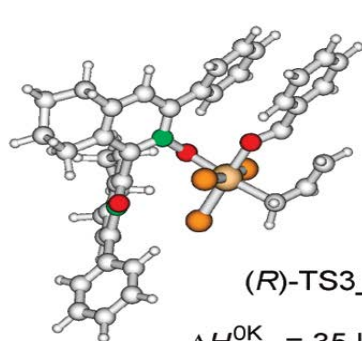
(R)-TS3_a

$\Delta H_{rel}^{0K} = 35$ kJ/mol

$\Delta H_{rel,TOL}^{298K} = 30$ kJ/mol
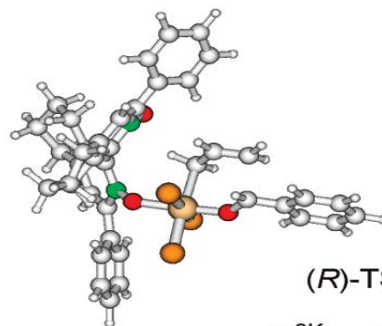
(R)-TS3_b

$\Delta H_{rel}^{0K} = 58$ kJ/mol

$\Delta H_{rel,TOL}^{298K} = 53$ kJ/mol
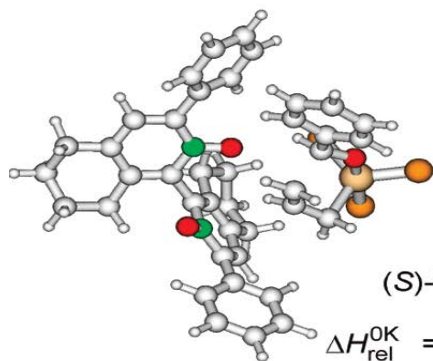
(S)-TS4_a

$\Delta H_{rel}^{0K} = 9$ kJ/mol

$\Delta H_{rel,TOL}^{298K} = 12$ kJ/mol
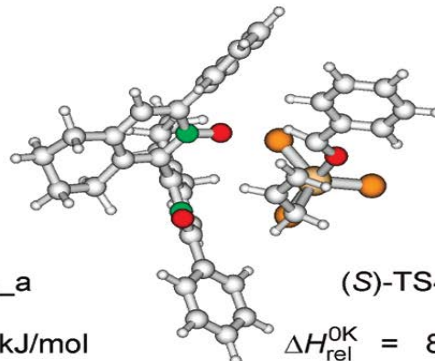
(S)-TS4_b

$\Delta H_{rel}^{0K} = 8$ kJ/mol

$\Delta H_{rel,TOL}^{298K} = 13$ kJ/mol

Ducháčková, L; Kadlčíková, A.; Kotora, M. ; Roithová, J.: Oxygen Superbases as Polar Binding Pockets in Nonpolar Solvents. *J. Am. Chem. Soc.* **2010**, *132*, 12660.

UOCHB AV ČR Computer Modeling of Chemical Reactions and Enzyme Catalysis

Asymmetric Allylation of Aldehydes with Allyltrichlorosilanes

Scheme 1. Allylation of aldehydes **1** with allyl and crotyl trichlorosilanes **2-4**.[a]

1a-m

2, R_E = H, R_Z = H
3, R_E = Me, R_Z = H
4, R_E = H, R_Z = Me

5

$(^+)^-$**9** (**METHOX**)

(S)-$(-)$-**9** (**Quinox**)

6, R_E = H, R_Z = H
7, R_E = Me, R_Z = H
8, R_E = H, R_Z = Me
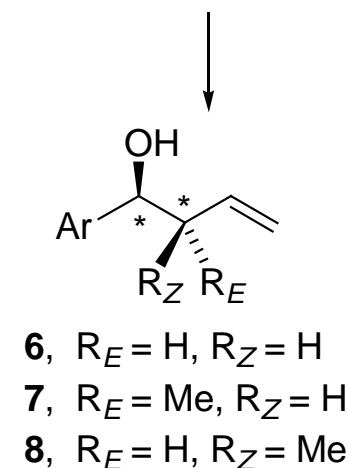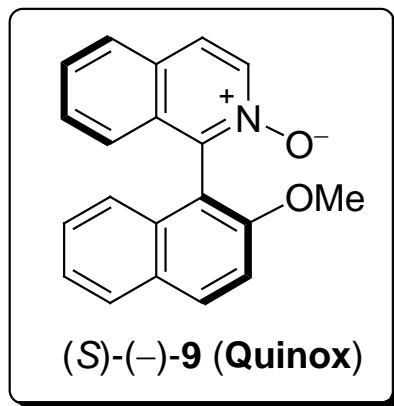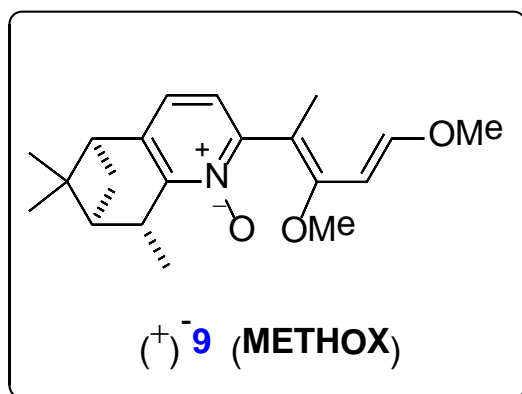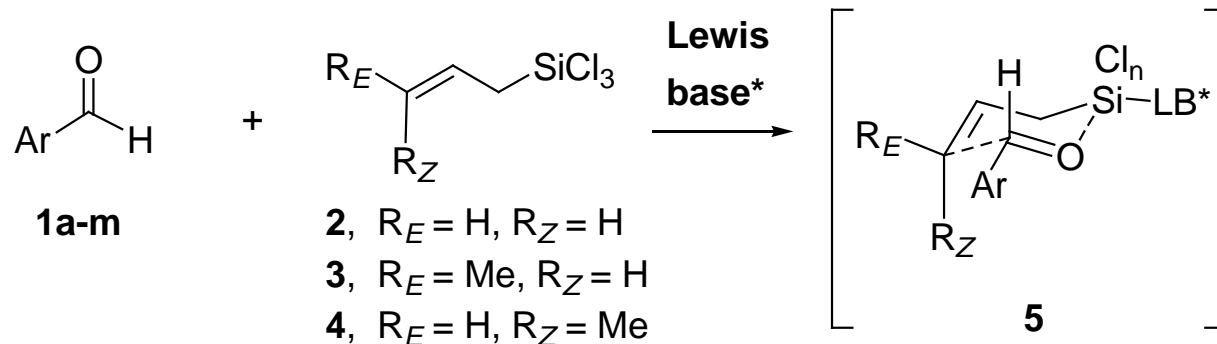
[a]For **a-m**, see Table 1.

Table: The Allylation of Aldehydes 1a-k with Allyltrichlorosilane 5a Catalyzed by Lewis Bases

Entry	Aldehyde	Ar	Catalyst (mol%)	Solvent	Temp (°C)	Time (h)	Yield (%)[b]	ee (%)[c,d]
1	1a	Ph	(+)-9 (5)	MeCN	-40	18	?95	96 (S)
2	1b	4-CF$_3$-C$_6$H$_4$	(+)-9 (5)	MeCN	-40	18	86	93 (S)
3	1c	4-MeO-C$_6$H$_4$	(+)-9 (5)	MeCN	-40	18	?95	96 (S)
4	1d	3-MeO-C$_6$H$_4$	(+)-9 (5)	MeCN	-40	18	87	95 (S)
5	1e	2-MeO-C$_6$H$_4$	(+)-9 (5)	MeCN	-40	18	?95	89 (S)
6	1f	4-Cl-C$_6$H$_4$	(+)-9 (5)	MeCN	-40	18	80	94 (S)
7	1g	3-Cl-C$_6$H$_4$	(+)-9 (5)	MeCN	-40	18	81	97 (S)
8	1h	2-Cl-C$_6$H$_4$	(+)-9 (5)	MeCN	-40	18	75	92 (S)
9	1i	3,5-Me$_2$-C$_6$H$_4$	(+)-9 (5)	MeCN	-40	18	0	–
10	1j	2,6-Me$_2$-C$_6$H$_4$	(+)-9 (5)	MeCN	-40	18	0	–
11	1a	Ph	(–)-15e (10)	CHCl$_3$	-40	18	60	90 (S)
12	1b	4-CF$_3$-C$_6$H$_4$	(–)-15e (10)	CHCl$_3$	-40	18	34	85 (S)
13	1c	4-MeO-C$_6$H$_4$	(–)-15e (10)	CHCl$_3$	-40	18	25	91 (S)
14	1e	2-MeO-C$_6$H$_4$	(–)-15e (10)	CHCl$_3$	-40	18	53	75 (S)
15	1f	4-Cl-C$_6$H$_4$	(–)-15e (10)	CHCl$_3$	-40	18	63	88 (S)
16	1g	3-Cl-C$_6$H$_4$	(–)-15e (10)	CHCl$_3$	-40	18	54	89 (S)
17	1h	2-Cl-C$_6$H$_4$	(–)-15e (10)	CHCl$_3$	-40	18	75	86 (S)
18	1i	3,5-Me$_2$-C$_6$H$_4$	(–)-15e (10)	MeCN	-20	18	0	?
19	1a	Ph	(+)-16 (5)	MeCN	-20	18	87	72 (S)[e]
20	1k	4-F-C$_6$H$_4$	(+)-16 (5)	MeCN	-20	18	58	70 (S)[e]
21	1c	4-MeO-C$_6$H$_4$	(+)-16 (5)	MeCN	-20	18	72	70 (S)[e]
22	1i	3,5-Me$_2$-C$_6$H$_4$	(+)-16 (5)	MeCN	-20	18	73	62 (S)[e]
23	1a	Ph	(+)-10 (5)	CH$_2$Cl$_2$	-40	2	68	87 (R)[f]
24	1b	4-CF$_3$-C$_6$H$_4$	(+)-10 (5)	CH$_2$Cl$_2$	-40	2	85	96 (R)[f]
25	1c	4-MeO-C$_6$H$_4$	(–)-10 (5)	CH$_2$Cl$_2$	-40	18	70	16 (S)[f,g]
26	1e	4-MeO-C$_6$H$_4$	(+)-10 (5)	CH$_2$Cl$_2$	-20	18	75	72 (R)
27	1e	4-MeO-C$_6$H$_4$	(+)-10 (5)	CH$_2$Cl$_2$	0	18	82	45 (R)
26	1d	3-MeO-C$_6$H$_4$	(+)-10 (5)	CH$_2$Cl$_2$	-40	12	73	80 (R)[f]
27	1e	2-MeO-C$_6$H$_4$	(+)-10 (5)	CH$_2$Cl$_2$	-40	12	40	37 (R)[f]
28	1i	3,5-Me$_2$-C$_6$H$_4$	(+)-10 (5)	CH$_2$Cl$_2$	-40	16	68	81 (R)[h]
29	1j	2,6-Me$_2$-C$_6$H$_4$	(+)-10 (5)	CH$_2$Cl$_2$	-40	18	0	–

"Non-catalysed" reaction
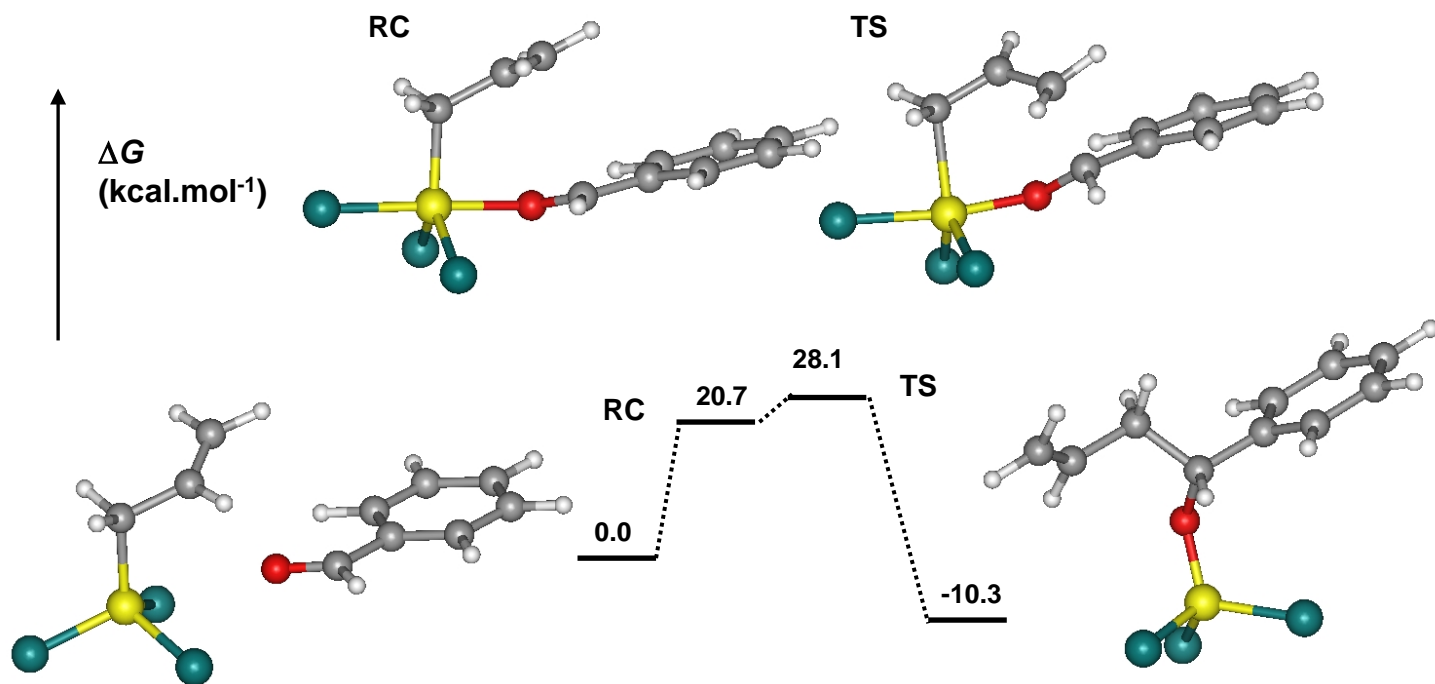
$\Delta E^{\ddagger} = 15.3$ **kcal.mol**$^{-1}$ **…CCSD(T)/aug-cc-pVDZ**
$\Delta E^{\ddagger} = 15.6$ **kcal.mol**$^{-1}$ **…RI-DFT(PBE)+D/TZVPP**

Pyridine-N-oxide: associative mechanism

ΔG
(kcal.mol^{-1})

RC

2.80

1.98

TS

2.21

2.05

PC

27.5

25.0

TS

RC

7.1

PC

0.0

-10.3
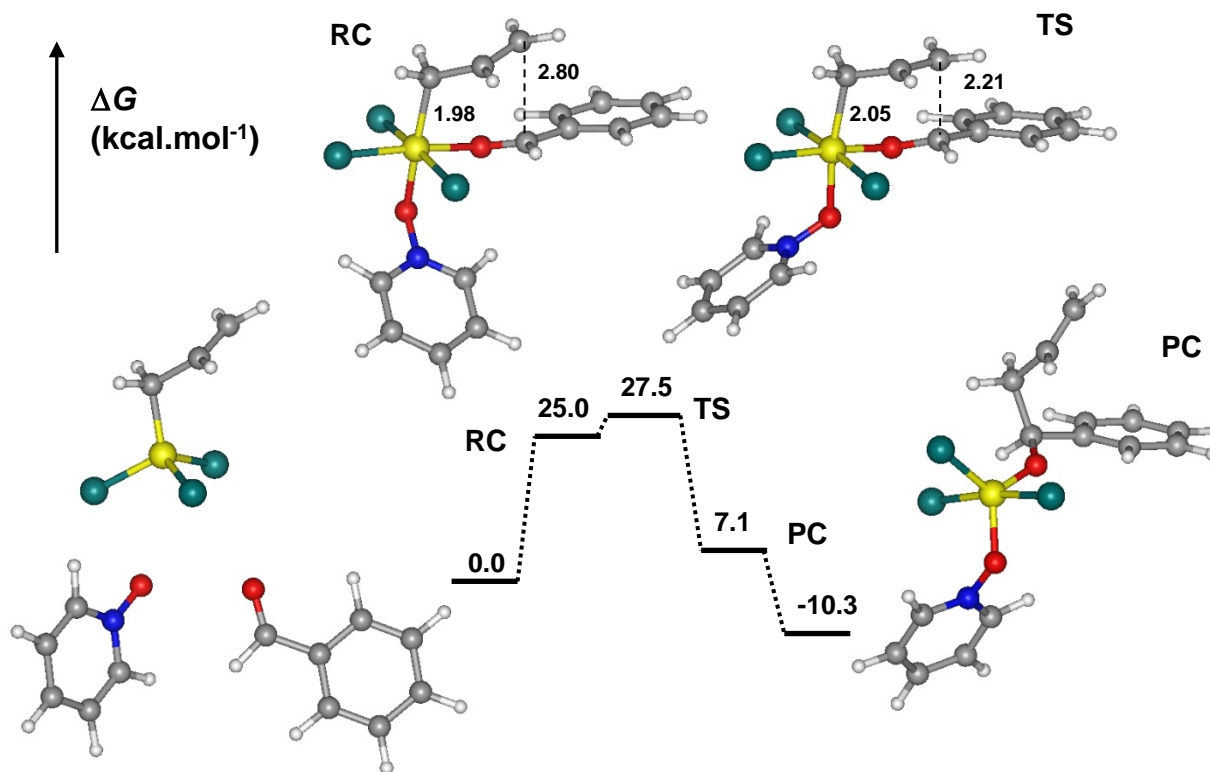
Second-sphere mechanism (ruled out)

QUINOX Catalyst

$(R)^-(^+)^-$**10** (**QUINOX**)
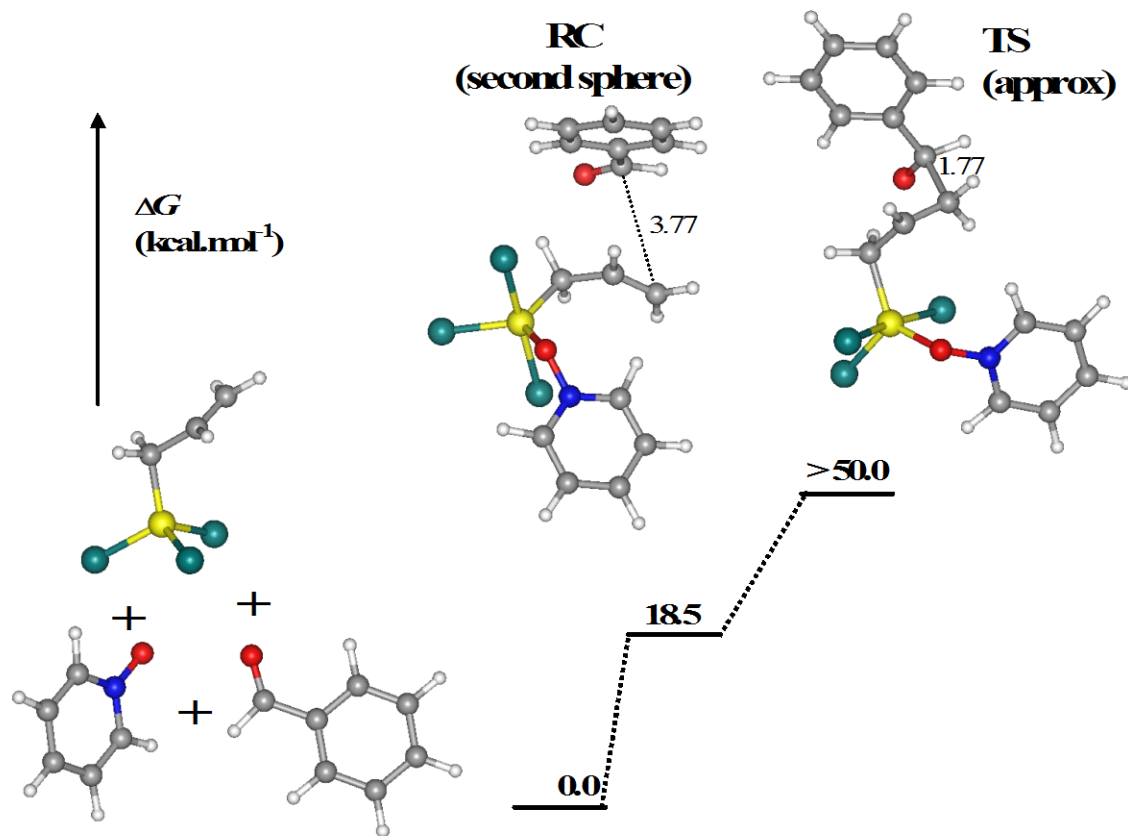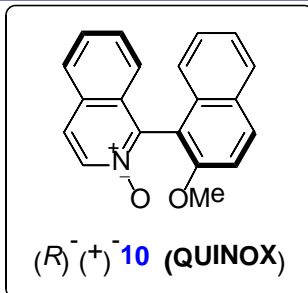
ee (calc) = 82%

ee (exp) = 87%
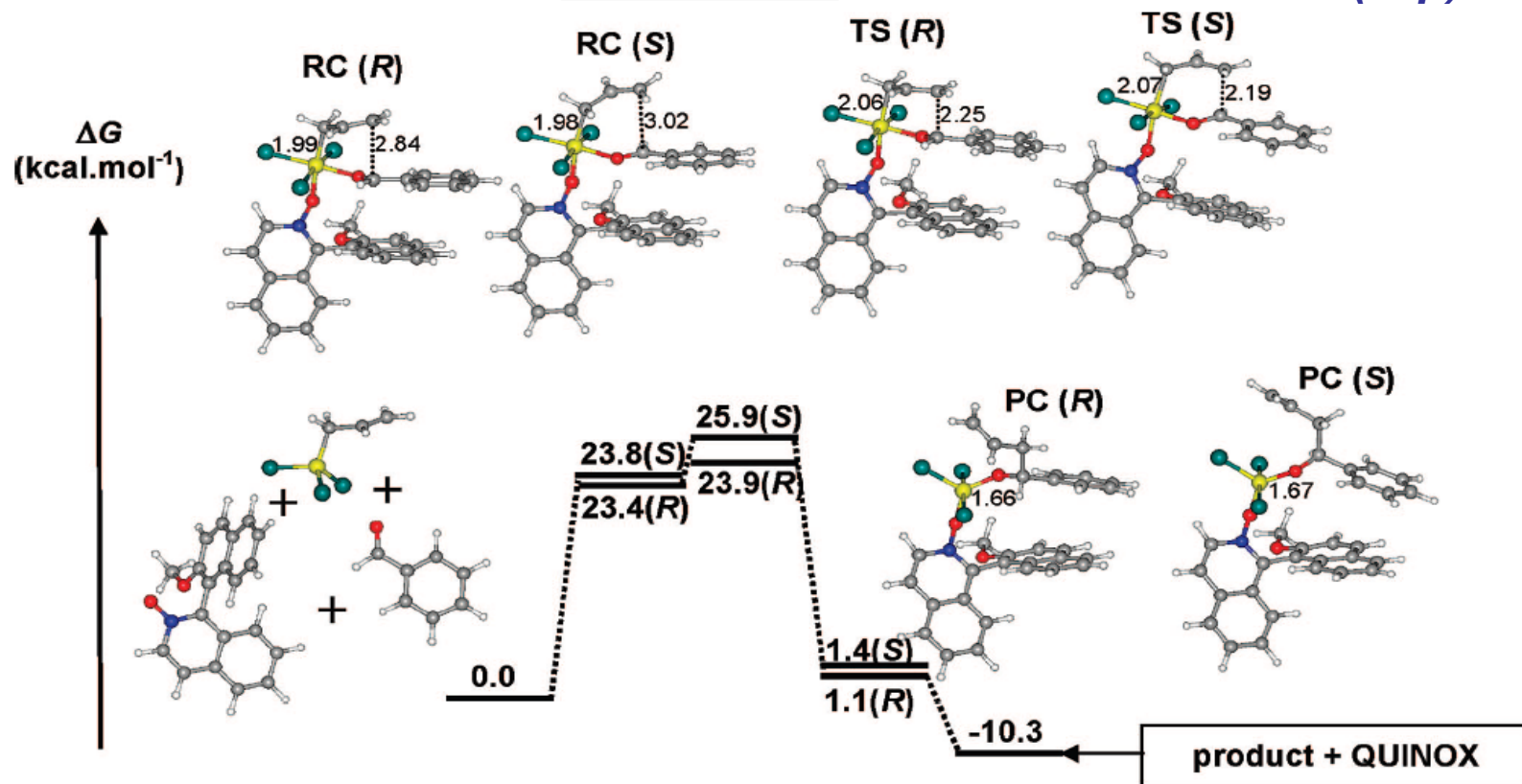
Figure 4. The equilibrium geometries of the most stable reactant complexes (RC), transition states (TS), and product complexes (PC) along the reaction coordinate for the associative pathway of allylation of benzaldehyde (**1a**) catalyzed by (R)-$(+)$-QUINOX (**9**). The calculated values for ΔG were obtained at the RI-PBE(+D)/TZVP//RI-PBE(+D)/6-31G(d) level; all distances are in Å.

Table: The calculated thermochemical data for METHOX as a catalyst. All values are in kcal.mol^{-1}.
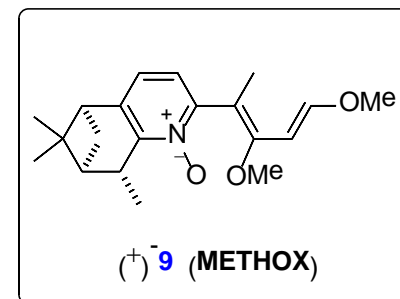
$(^+)^-$**9** (**METHOX**)

mechanism	config.	reactant complex	transition state	product complex
associative	R	24.4	29.3	-2.0
	S	-^{a}	28.7	-4.8
dissociative	R	25.0	25.6	-2.0
	S	17.8	23.3	-4.8

ee (calc) = 88%

ee (exp) = 96%

METHOX Catalyst
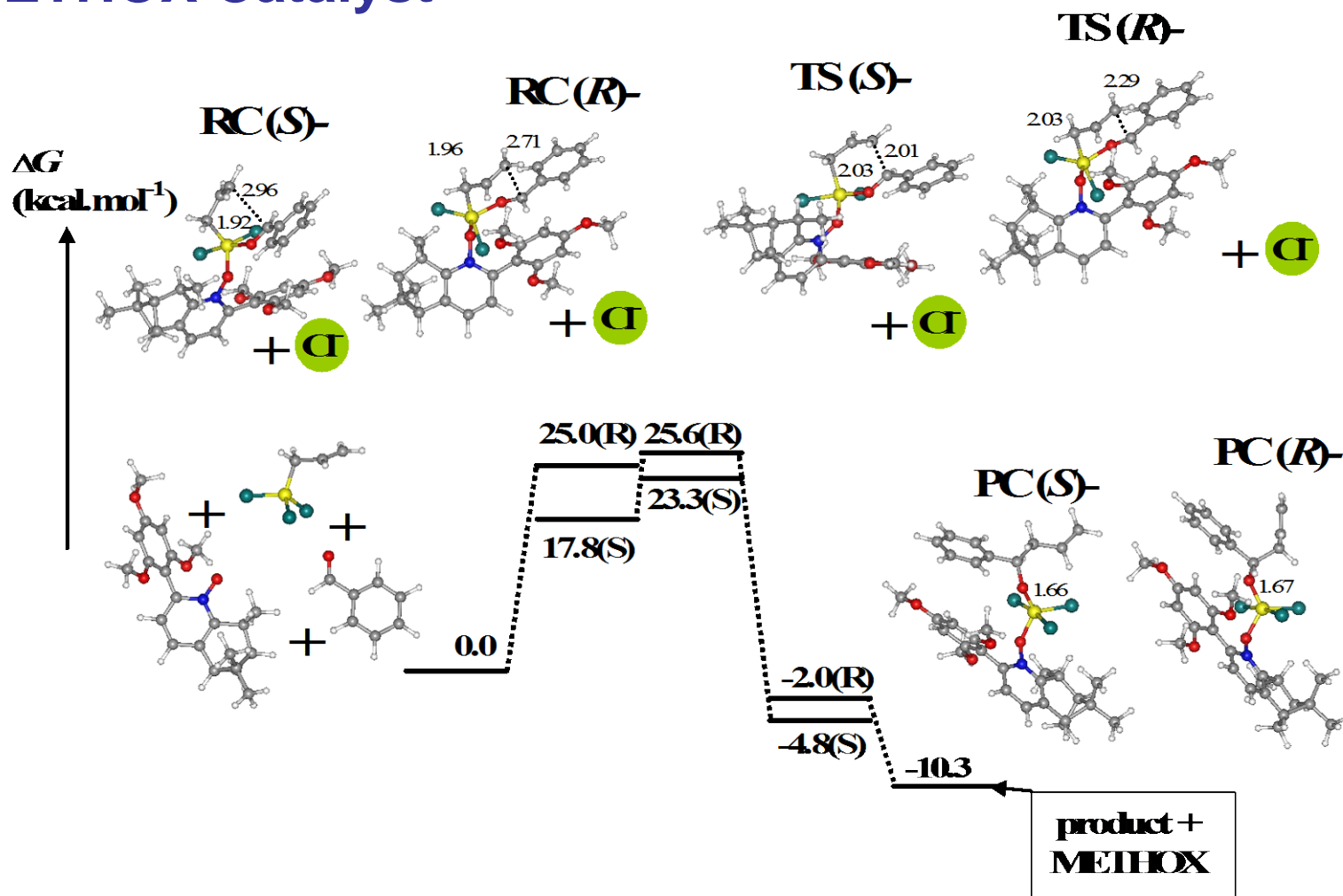
Malkov, A. V.; Stončius, S.; Bell, M.; Castelluzzo, F.; Ramírez-López, P.; Biedermannová, L.; Langer, V.; Rulíšek, L.; Kočovský, P.: *Chem. Eur. J.* **2013**, *19*, 9167-9185.

Origin of the stereoselectivity

Table: The decomposition of the free energy barriers into the contributions originating in zero-point energy corrections, entropy, solvation energies, and dispersion energies. All values are in kcal.mol^{-1}.

Catalyst	config	$\Delta E_{gp}{}^{a}$	$\Delta G_{solv}{}^{b}$	$\Delta(-T\Delta S)_{gp}{}^{c}$	$\Delta E_{disp}{}^{d}$
QUINOX	*R*	0.0	0.0	0.0	0.0
(associative TS)	*S*	-0.3	0.7	0.5	1.1
METHOX	*R*	0.0	0.0	0.0	0.0
(dissociative TS)	*S*	-3.2	-0.4	-0.6	1.9

[a] ΔE_{gp} is the difference in the *in vacuo* energies between R, S isomers
[b] ΔG_{solv} is the difference in solvation free energies between R, S isomers
[c] $\Delta(-T\Delta S)_{gp}$ is the difference in the *in vacuo* entropic terms between R, S isomers
[d] ΔE_{disp} is the difference in the dispersion energy stabilizations between R, S isomers

Mechanistic Dichotomy in the Asymmetric Allylation of Aldehydes with Allyltrichlorosilanes Catalyzed by Chiral Pyridine *N*-Oxides

Scheme 5. Mechanism of catalysls by chiral pyridine-*N*-oxides

Stereoselectivities quantitatively predicted (within 1 kcal.mol^{-1})
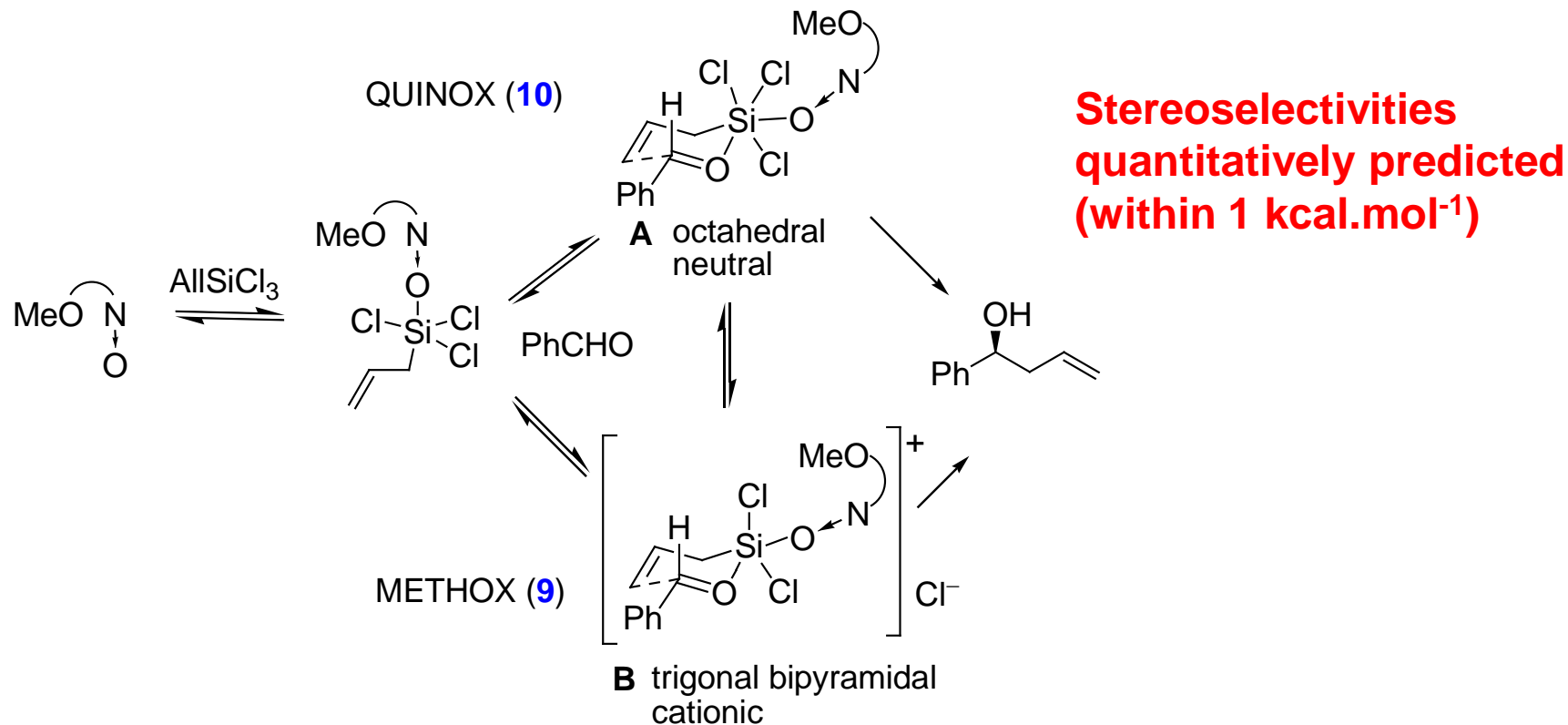
Malkov, A. V.; Ramírez-López, P.; Biedermannová, L.; Rulíšek, L.; Dufková, L.; Kotora, M.; Zhu, F.; Kočovský, P.: *J. Am. Chem. Soc.* **2008**, *130*, 5341. Malkov, A. V.; Stončius, S.; Bell, M.; Castelluzzo, F.; Ramírez-López, P.; Biedermannová, L.; Langer, V.; Rulíšek, L.; Kočovský, P.: *Chem. Eur. J.* **2013**, *19*, 9167.

Summary and Outlook

Conformational complexity (competing reaction pathways)
Entropic effects (ideal gas + PCM solvation = ??, *Cl⁻ translational entropy*)
Solvation Effects (non-innocent solvents, ionic systems, COSMO-RS)
Accuracy of TS barriers (2 kcal.mol^{-1} is optimistic error bar in medium-sized, well-defined models, while it can easily overcome 5 kcal.mol^{-1} in more complex systems)
…tunneling, "non-TST" systems,…

En Route **from Quantitative Insight to Simpler Concepts?**

Qualitative Concepts (60's – 80's)

Towards Accurate Numbers (90's -2012)

Quantitative Concepts (and Guidance for Experiments??)

Copper(II) and Zinc(II) Complexes of Conformationally Constrained Polyazamacrocycles as Efficient Catalysts for RNA Model Substrate Cleavage in Aqueous Solution at Physiological pH

Daniel Bím,[a, b] Eva Svobodová,[a] Václav Eigner,[c] Lubomír Rulíšek,*[b] and Jana Hodačová*[a]
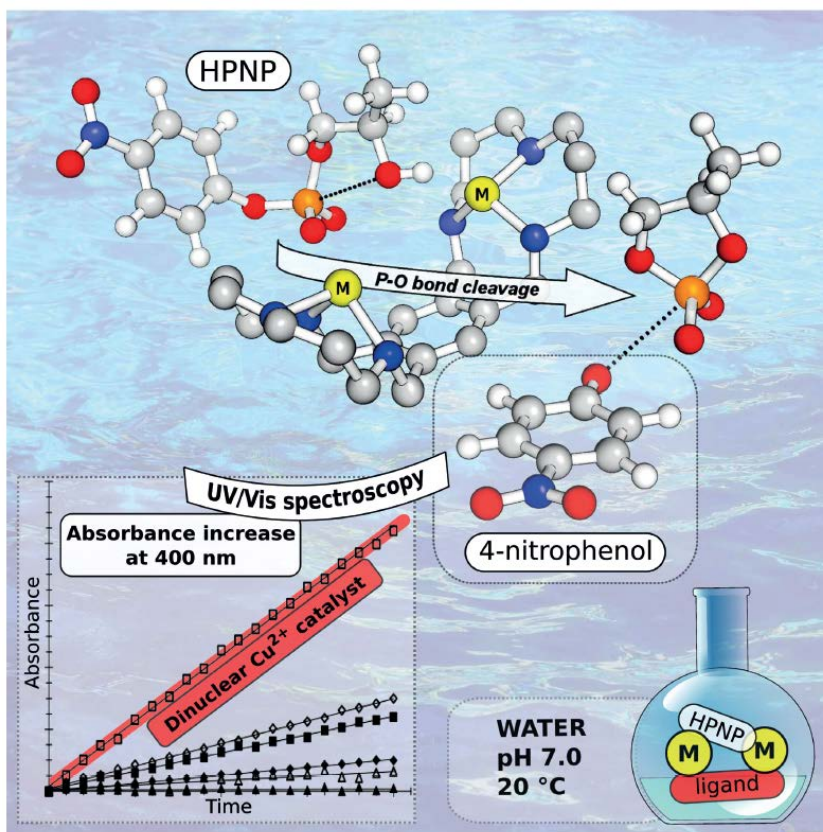
Computer Modeling of Chemical Reactions and Enzyme Catalysis
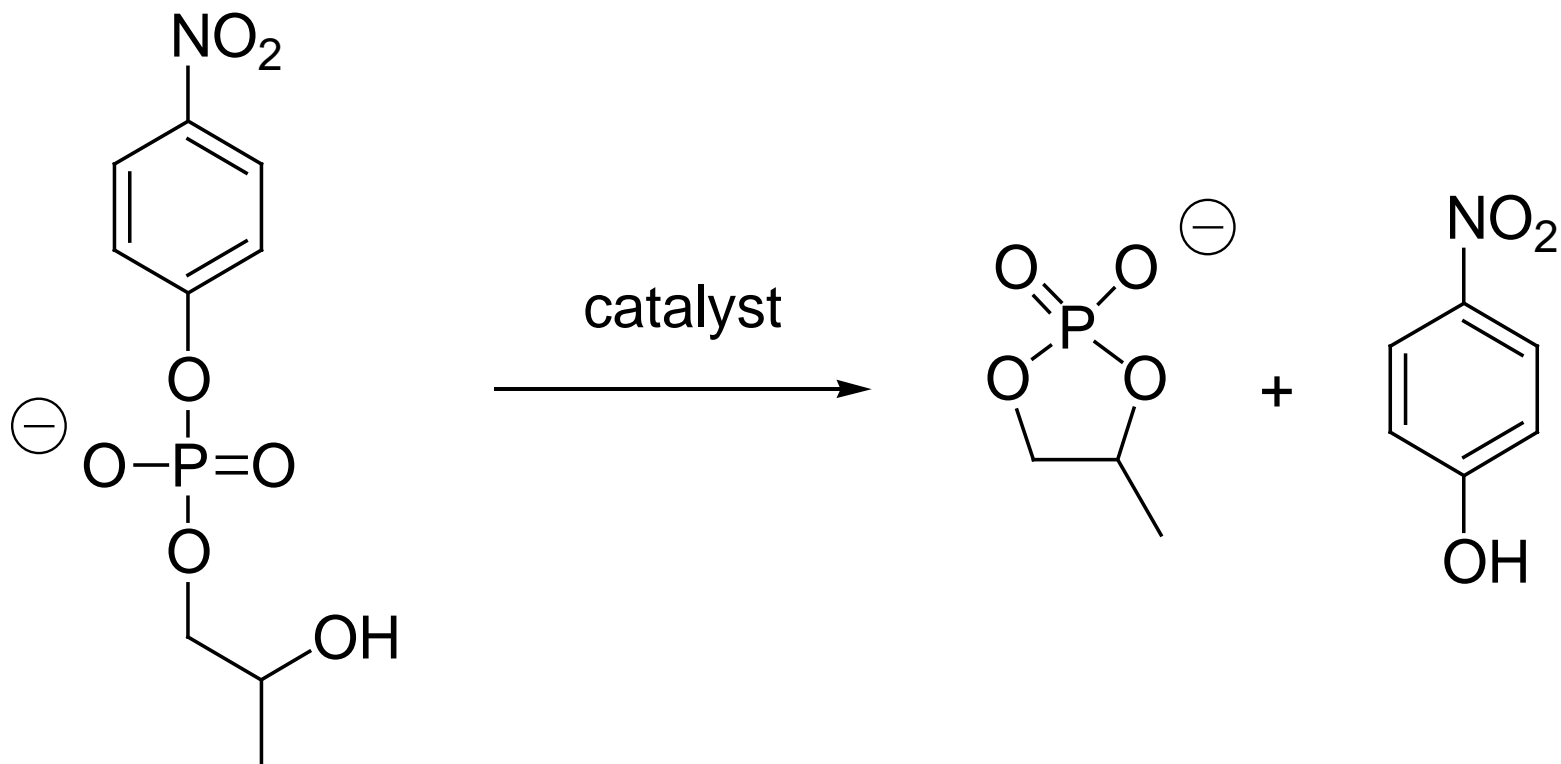
Scheme. Cleavage of hydroxypropyl-4-nitrophenylphosphate (HPNP)

- Phosphate diester linkage: RNA, DNA, and cGMP
- extremely stable towards hydrolytic cleavage under physiological conditions, half-lives 100 years for RNA, up to millions of years for DNA.
- Specific nucleases are able to accelerate the rate of hydrolysis of the P–O bond by a factor of up to 10^{17}

Catalyst

1

2

Reactant Complex

ÚOCHB AV ČR
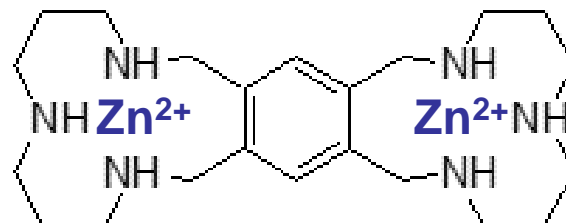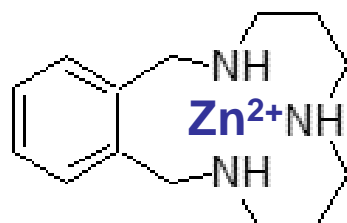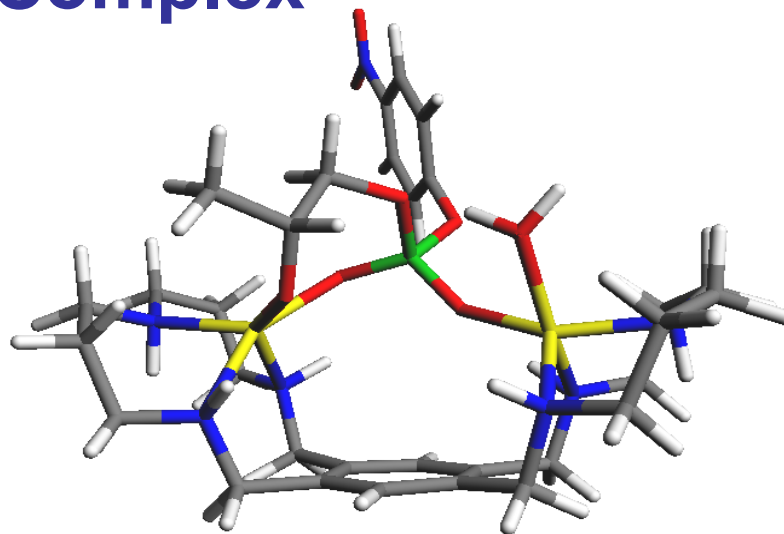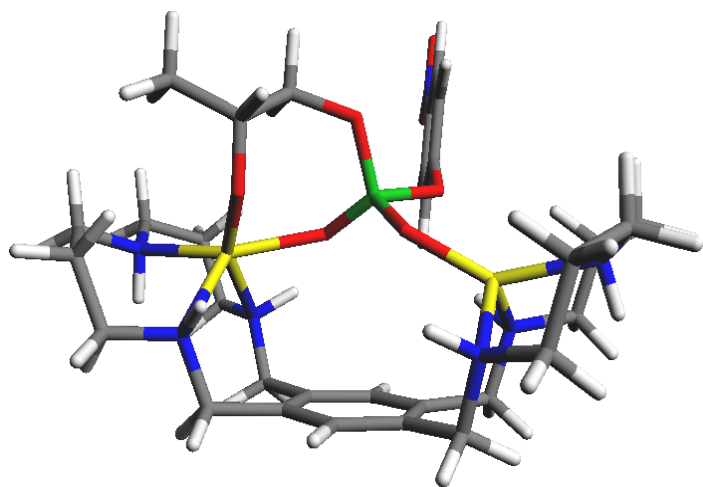
Experimental data
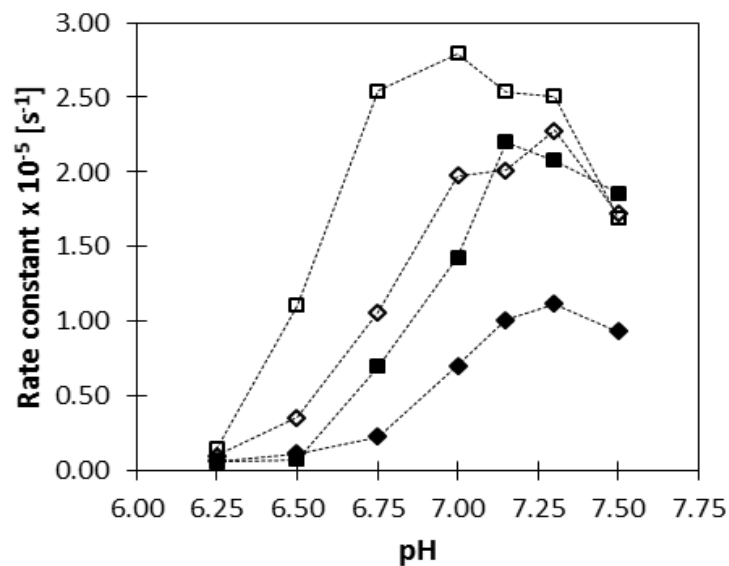
Table 2. Michaelis–Menten parameters for HPNP cleavage in 10 mM aqueous HEPES buffer at pH 7.0 catalyzed by the copper(II) and zinc(II) complexes of ligands **1** and **2** at 20 °C.

Catalyst	V_{max} [M·s^{-1}] [a]	K_M [M] [a]	K_{ass} [M^{-1}] [b]	k_{cat} [s^{-1}] [c]
Cu-**1**	1.14×10^{-7}	0.0103	97	5.68×10^{-4}
Zn-**1**	5.39×10^{-8}	0.0184	54	2.69×10^{-4}
Cu$_2$-**2**	1.75×10^{-7}	0.00777	129	8.73×10^{-4}
Zn$_2$-**2**	3.24×10^{-8}	0.00701	143	1.62×10^{-4}

ÚOCHB AV ČR

Reaction Coordinate (S$_N$2)
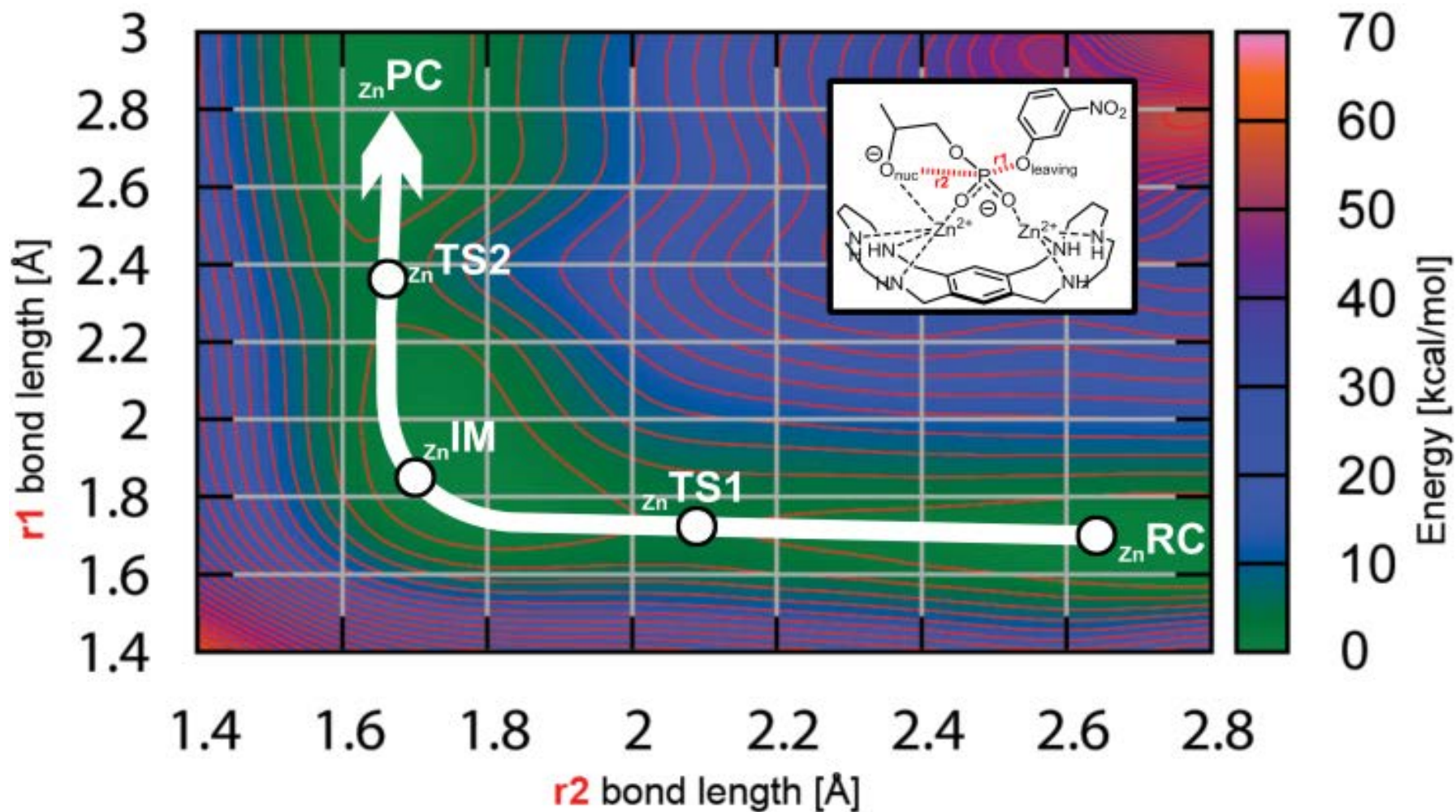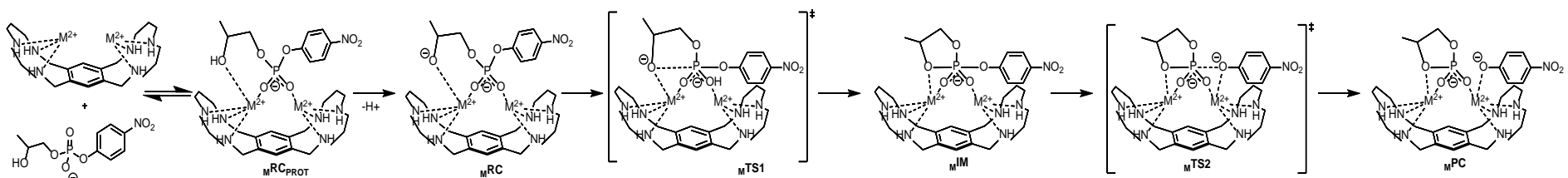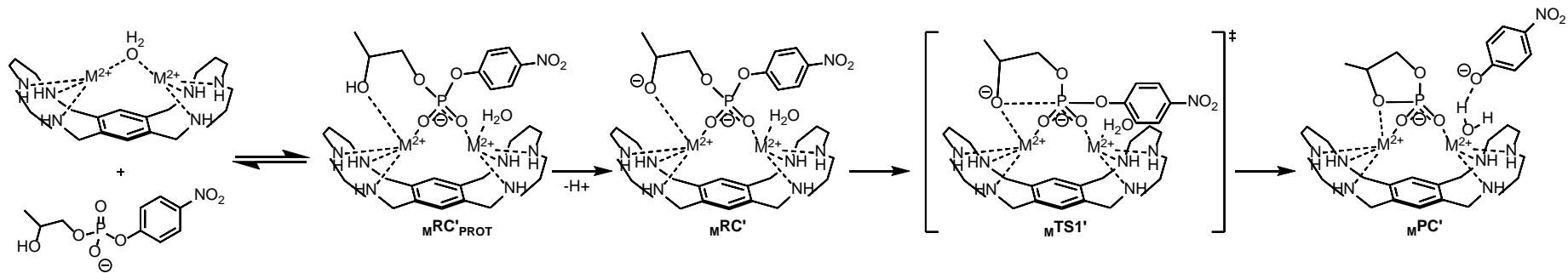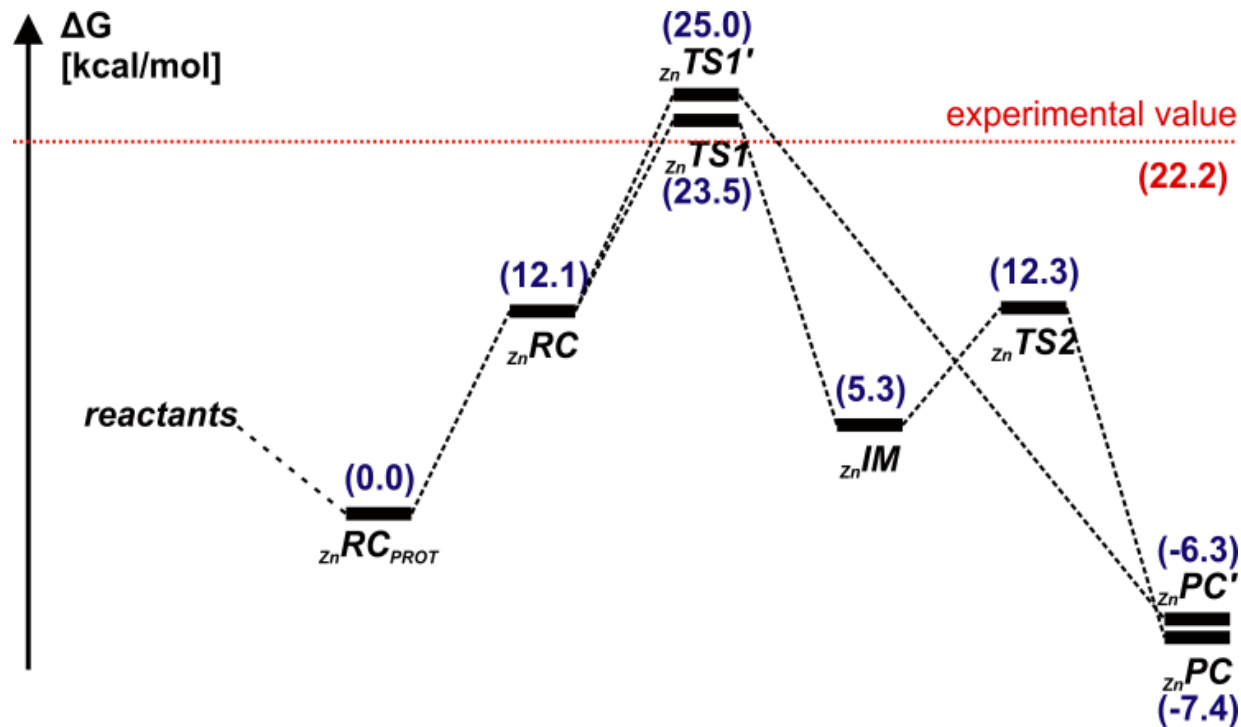
Figure. Energy diagram for the proposed reaction mechanisms with the Zn_2-2 catalyst. All Gibbs free energy values are in kcal mol^{-1} and were calculated with inclusion of solvation effects using the COSMO-RS solvation model. The presented values were obtained using the PBE0 functional
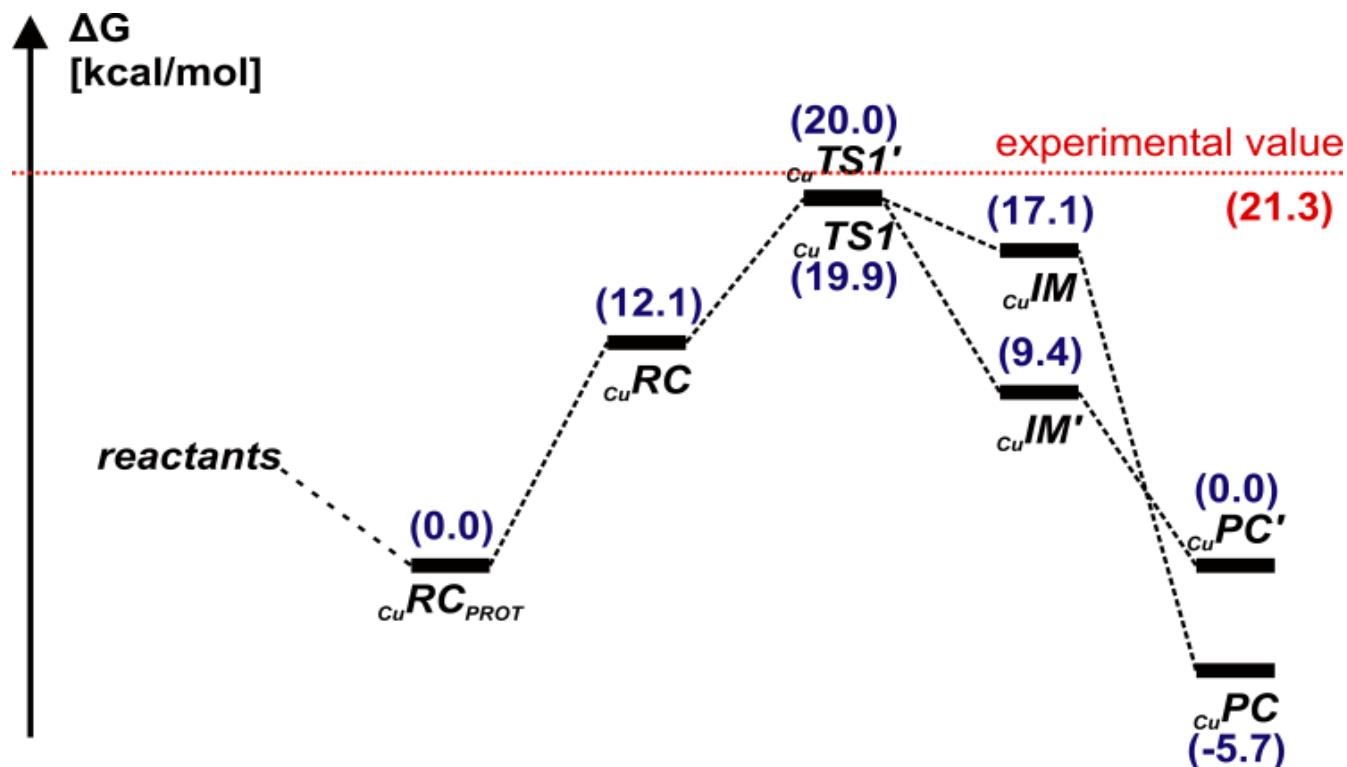
Figure. Energy diagram for the proposed reaction mechanisms with the Cu_2-2 catalyst. All Gibbs free energy values are in kcal mol^{-1} and were calculated with inclusion of solvation effects using the COSMO-RS solvation model. The presented values were obtained using the PBE0 functional